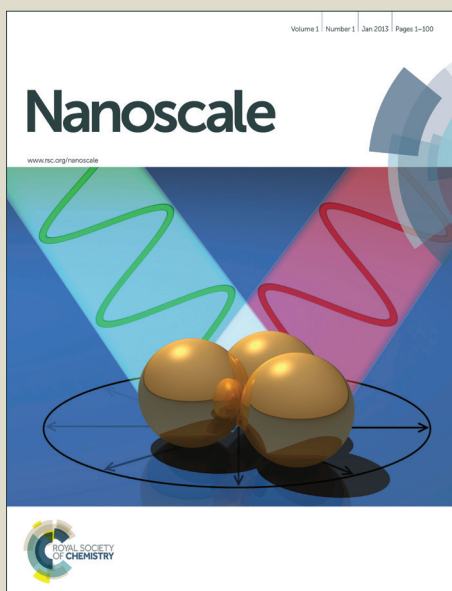


Nanoscale

Accepted Manuscript



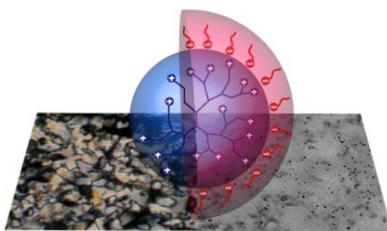
This is an *Accepted Manuscript*, which has been through the Royal Society of Chemistry peer review process and has been accepted for publication.

Accepted Manuscripts are published online shortly after acceptance, before technical editing, formatting and proof reading. Using this free service, authors can make their results available to the community, in citable form, before we publish the edited article. We will replace this *Accepted Manuscript* with the edited and formatted *Advance Article* as soon as it is available.

You can find more information about *Accepted Manuscripts* in the [Information for Authors](#).

Please note that technical editing may introduce minor changes to the text and/or graphics, which may alter content. The journal's standard [Terms & Conditions](#) and the [Ethical guidelines](#) still apply. In no event shall the Royal Society of Chemistry be held responsible for any errors or omissions in this *Accepted Manuscript* or any consequences arising from the use of any information it contains.

Graphical abstract



Short sentence

Mesomorphic hyperbranched polymers comprising ionic functionalities allow the formation of controlled-size nanoparticles thanks to strong interactions with inorganic materials precursors.

Cite this: DOI: 10.1039/c0xx00000x

www.rsc.org/xxxxxx

PAPER

Mesomorphic Ionic Hyperbranched Polymers: Effect of Structural Parameters on Liquid-Crystalline Properties and on the Formation of Gold Nanohybrids

Hong Hanh Nguyen,^{a,b} Clara Valverde Serrano,^c Pierre Lavedan,^d Dominique Goudounèche,^e Anne-Françoise Mingotaud,^{a,b} Nancy Lauth-de Viguerie,^{a,b,*} Jean-Daniel Marty^{a,b,*}

Received (in XXX, XXX) Xth XXXXXXXXX 20XX, Accepted Xth XXXXXXXXX 20XX

DOI: 10.1039/b000000x

ABSTRACT: Branched thermotropic liquid crystals were successfully obtained from ionic interactions between hyperbranched polyamidoamine and sodium dodecylsulfate. These complexes present columnar rectangular and lamellar thermotropic mesophases as demonstrated by polarizing optical microscopy, differential scanning calorimetry, and small-angle X-ray scattering. The relationship between the structural characteristics of the polymers (size of the hyperbranched core, hyperbranched or dendritic nature of the core, substitution ratio) and the mesomorphic properties were studied. *In situ* formation of gold nanoparticles was then performed. The templating effect of the liquid crystal mesophase resulted in the formation of isotropic nanoparticles, the size of which was dictated by the local organization of the mesophase and by the molar mass of the hyperbranched complex.

1. Introduction

In recent years, tremendous research efforts to develop nanoscale organic/inorganic building blocks with well controlled morphology and to define efficient self-assembly protocols to get access to functional materials have been described in literature. In this context, intimate mixtures of liquid crystals (lyotropic or thermotropic) and nanoparticles have aroused great interest in the scientific community.¹⁻³ If most described studies involved the mixing of preformed nanoparticles (NPs) within liquid crystals, literature reveals particularly interesting attempts in synthesizing NPs within mesophases of liquid crystals.^{2,4} For instance, ZnSe nanomaterials have been synthesized in lyotropic systems based on amphiphilic triblock copolymers. Depending on the liquid crystalline state, quantum dots, nanodisks or even nanowires could be obtained.^{5,6} Nanoporous materials (generally silica) have also been fabricated via true liquid crystal templating.⁷ Whereas the large majority of such research employs lyotropic liquid crystals, very few publications deal with the elaboration of nanomaterials within thermotropic ones.⁸⁻¹⁵ Indeed, the development of an *in situ* procedure to generate NPs within a thermotropic liquid crystalline (LC) medium has proved to be quite a challenging task mainly due to diffusion hindrance of reactants in such medium. Most studies involve the *in situ* reduction of metal precursors via oxidation of the LC medium in order to obtain the desired NPs. For instance, the formation of CuCl nanostructures inside a mixture of an ionic liquid and a derivative of ascorbic acid has been reported.^{13,14} This resulted in the formation of CuCl nanoplatelets with a relatively uniform thickness of about 220 nm and in-plane sizes of 5-50 nm. Glass-

forming liquid crystalline materials acting as a reducing agent were also used to obtain gold NPs whose size and shape depended on both the amount of precursor content and the LC state.¹⁰ Isotropic NPs of gold or silver have also been synthesized by heating LC materials doped with the corresponding metal salts.⁹ In other cases, sputtering¹⁵ or electrodeposition⁸ techniques were used to form NPs in thermotropic systems. Recently, we reported the use of a thermotropic liquid crystal branched and hyperbranched polymers obtained from the grafting of LC moiety on a branched core for such a purpose.^{11,12} To avoid disruption of the liquid crystalline mesophase during NPs formation, this approach involves the *in situ* hydrolysis of dicyclohexylzinc, [Zn(Cy₂)] leading to ZnO NPs with volatile cyclohexane as the only side product.¹⁶ We demonstrated a direct correlation between the structural characteristics of the LC, the type of organization implicated during NPs synthesis and the morphology of the nanostructures obtained. Whereas in isotropic conditions only isotropic NPs were obtained, experiments performed in the nematic phase state of the LC compound led to the formation of anisotropic ZnO structures.^{11,12} Thus, nano-worm-like or nano-wire structures were grown in branched¹¹ and hyperbranched liquid crystals.¹⁰

Mesomorphic dendritic polymers appear thus as good candidates for the synthesis of nanohybrids. Moreover, interactions of the organic structure with metal precursor appear as a key parameter to control their morphology. In this context, the use of LC branched polymer exhibiting an ionic part could be of special interest to study the effect of the mesophase nature on the NPs growth. Indeed, these ionic structures facilitate interactions with ionic metal precursor and thus insure the homogeneity of hybrid materials. Moreover, their specific

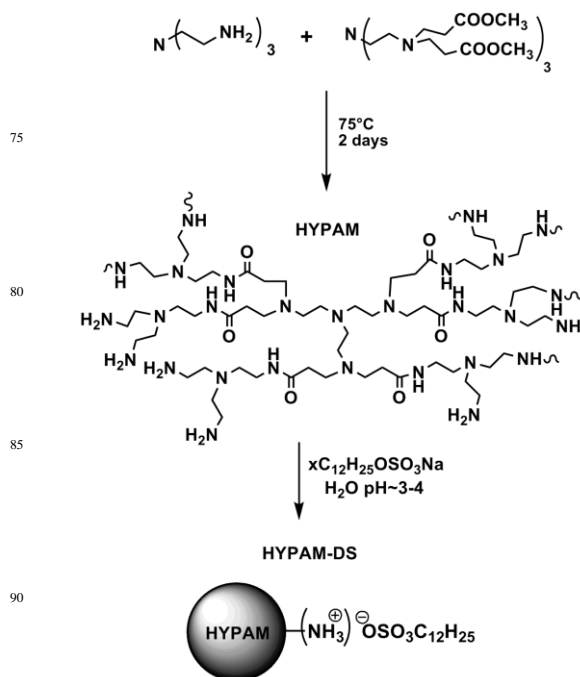
organization (mainly lamellar) could induce specific diffusion phenomena that could be taken into account to modulate NPs growth mechanism. In the past few years, LC dendritic structures made of components interacting by means of ionic interactions have attracted great interest: they do not necessitate tedious synthetic procedures like dendritic structures obtained by means of covalent bonds between a dendritic core and a LC group. In addition, the nature of the external functional group can be easily tuned. This strategy has been well described in the case of amine-terminated dendritic structures complexed with different carboxylic acids exhibiting or not LC properties.¹⁷⁻³⁰ Ionic LC dendrimers based on polyethyleneimine (PEI),^{25,29,30} poly(propylene imine) (PPI)^{18, 20-22, 24, 26-28} and poly(amidoamine) (PAMAM)^{17,19,23,25} dendrimers have been especially studied. They exhibited mesophases of different nature depending mainly on the generation and chemical nature of the hyperbranched core and on the structure of the alkyl chain of the carboxylic acid (number of alkyl chain per acid or introduction of fluorinated moieties). Smectic A or square and hexagonal columnar mesophases were thus observed. If most of those studies focused on the use of well-defined dendrimers cores, ionic LC hyperbranched structures have not been thoroughly studied.^{25, 31, 32}

In this work, in a first part, the synthesis of a new family of thermotropic dendritic polymers comprising a hyperbranched polyamidoamine core (HYPAM-(NH₂)_n)^{33,34} and a dodecylsulfate-based shell based on non-covalent concept is described. The liquid crystalline properties of these core-shell architectures are thoroughly investigated by means of polarizing optical microscopy (POM), differential scanning calorimetry (DSC), and small-angle X-ray scattering (SAXS). The relationship between the structural characteristics of the polymers (size of the hyperbranched core, hyperbranched or dendritic nature of the core, substitution ratio) and the mesomorphic properties were closely investigated. Organizations as large aggregates in aqueous solutions of those polymers obtained from dilution of mesomorphic structures were also evidenced. In a second part, we highlighted how those thermotropic structures comprising ionic counterpart can be taken in account to interact in a homogeneous way with ionic salts. Interestingly, diffusion of dihydrogene inside those mesomorphic structures allowed the *in situ* formation of gold NPs within the liquid-crystalline phase. The effect of polymer structure and organization on the morphology of gold nanoparticles is then evaluated.

2. Results and discussion

2.1. Synthesis and characterization of the hyperbranched-dodecyl sulfate complexes. The synthesis of the hyperbranched polymers complexes is outlined in Scheme 1. Hyperbranched polyamidoamine cores with a structure similar to the one of PAMAM dendrimers were synthesized following a previously published procedure.³⁵⁻³⁷ Tris(2-aminoethyl)amine was reacted with tris(2-di(methylacrylate)aminoethyl)amine leading in a single step to hyperbranched structures. Their molar mass was evaluated by size exclusion chromatography (SEC) in carbonate buffer at pH 10 equipped with refractive index and light scattering detectors. A typical chromatogram is presented in supporting information (Figure S1). Calculated mass average

molar masses and dispersities are summarized in Table 1. Molar masses of the polymers were easily adjusted by changing the ratio between the hexaester and the triamine. Molar ratios close to 12:1, 10:1, or 8:1 led to polymers with molecular weight close to those of PAMAM of the third, fourth, and fifth generation, respectively. These hyperbranched polymers were therefore named HYPAM3, HYPAM4 or HYPAM5. Quantification of amine groups present in HYPAM structures were obtained from quantitative ¹³C NMR using Me₄NOH as a calibration compound (see Figure S2 in ESI). Results are reported in Table 1.³⁴ As expected, the number of primary amines for HYPAM and PAMAM polymers of similar molar mass were close regardless of the structure (see Table 1).



Scheme 1. Synthesis of hyperbranched polyamidoamines HYPAM and HYPAM-dodecyl sulfate (HYPAM-DS) complexes.

Table 1. Characteristics of Polymer Samples: Mass-average Molar Mass (\overline{M}_w), Dispersity (\mathcal{D}) and Primary Amine Content.

Sample	Triamine/hexaester ratio	\overline{M}_w *	\mathcal{D} *	Primary amines (mmol.g ⁻¹)**
HYPAM3	12	5200	1.4	5.0
PAMAM3	-	6900	n.d.	4.6
HYPAM4	10	13000	2.0	6.2
PAMAM4	-	14000	n.d.	4.5
HYPAM5	8	27000	2.3	4.2
PAMAM5	-	28000	n.d.	4.4

* Mass-average molar mass and dispersity index (\mathcal{D}) determined by LS-SEC.** Values obtained from quantitative ¹³C NMR experiments. Abbreviations: n.d.: not determined.

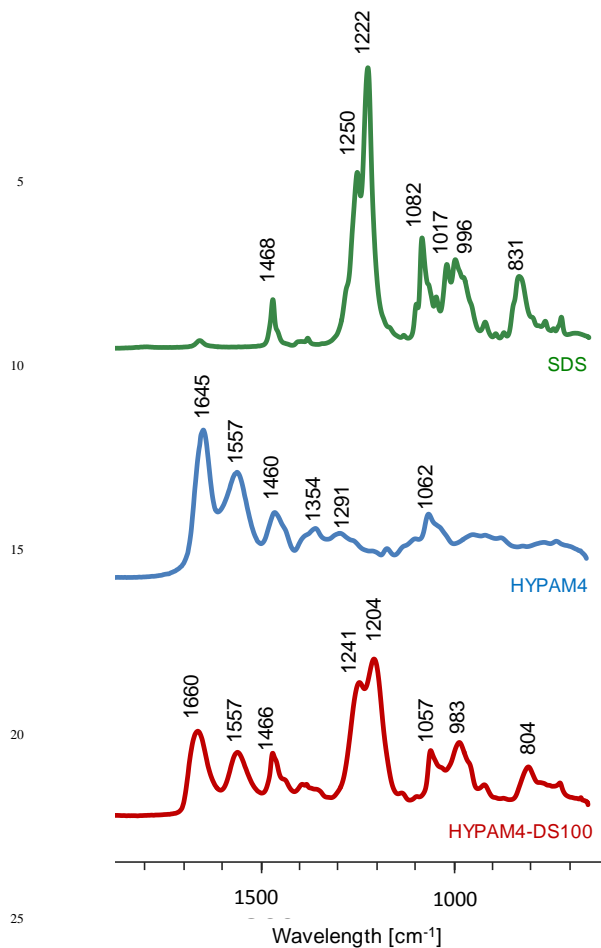


Figure 1. ATR-FTIR spectra of HYPAM4, SDS and of HYPAM4-DS100 complex at 25 °C (lamellar phase).

Amino-terminated HYPAMs cores were subsequently modified by dodecylsulfate (DS) moieties leading to the formation of HYPAM-DS complexes. For this, a dilute aqueous solution of sodium dodecylsulfate (SDS) was added to an aqueous solution of HYPAM at pH 3-4 adapting a procedure used by Canilho *et al.*³² The complex was obtained as a precipitate and the excess of sodium chloride salt was removed by washing with water. The small excess of non-interacting DS ligands, evidenced by the presence of thin peaks in ¹H NMR, was removed by dissolution of the precipitate in DMSO followed by reprecipitation in water.

ATR-FTIR spectroscopy was used to confirm the interactions between HYPAM and DS moieties. This is illustrated on the FTIR spectrum of HYPAM4 with a 100% level of functionalization of primary amine in Figure 1 and Figure S3 in ESI at 25°C (*i.e.* in the lamellar phase, *vide infra*). The formation of the ionic complex was confirmed by the shift of the two S=O asymmetric stretching bands of sulfate group from 1250 cm⁻¹ and 1222 cm⁻¹ to 1241 cm⁻¹ and 1204 cm⁻¹ respectively. In addition, the decrease in frequency of the symmetric S=O stretching band, from 1082 cm⁻¹ to 1057 cm⁻¹ can be interpreted as a change of counterion.³⁸ The vibration bands of carbonyl and amine groups of HYPAM at 1645 cm⁻¹ are also shifted to 1660 cm⁻¹ in the complex. Moreover, the complex was fully soluble in THF and CHCl₃, two solvents in which neither HYPAM nor SDS are. The

existence of interactions between HYPAM and DS moieties was further evidenced by NMR techniques in those solvents. A broadening of the signals corresponding to DS was observed on the ¹H NMR spectrum (Figure 2a). This was expected for DS in strong interaction with a macromolecule. To confirm this, a 1D NOE NMR experiment was performed by selectively irradiating the methylene protons in the α position of the sulfate function of DS (Figure S4 in ESI). A negative NOE effect was observed on both protons of the HYPAM core and the DS hydrophobic chain in the presence of the HYPAM core (Figure 2c). A control experiment was performed on acidified SDS (Figure 2b) (as mentioned before, SDS is not soluble in CHCl₃). In this case, a positive NOE effect on the vicinal protons was observed. This confirmed the strong interaction of HYPAM with DS. Indeed, macromolecules like HYPAM exhibit negative NOE effect with a fast build-up rate, while low-molecular weight DS has positive NOE signals with a slow build-up rate. When DS binds to HYPAM, it gains motional correlation time of the macromolecules, thus developing a negative NOE in the bound state. This negative intramolecular trNOE signals of DS indicates that those chains are in interaction with HYPAM core. This was confirmed by the presence of negative trNOE signals for the protons characteristic of the HYPAM core. The long mixing times used here (800 ms) generate pseudo-cross-peaks attributed to spin diffusion and magnetization transfer and thus explain the appearance of such an effect for all protons of the core. From both FTIR results in bulk and NMR experiments in solution an interaction may be assumed between HYPAM and DS chains. Those interactions likely arise from ionic interactions between sulfate group and protonated amine groups of the HYPAM hyperbranched core.³²

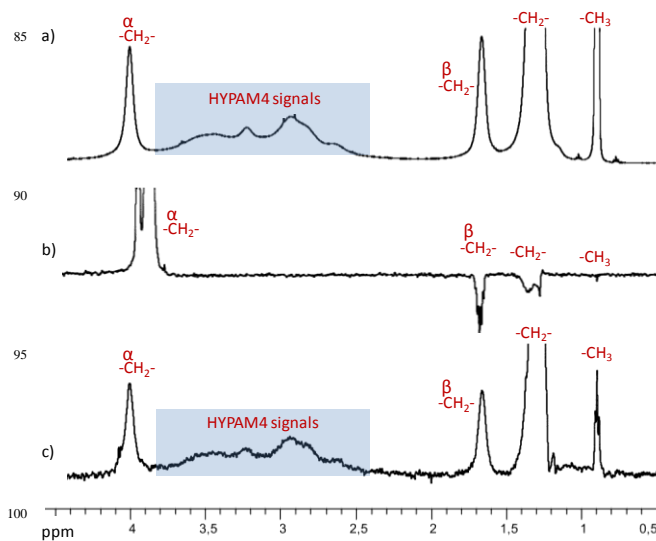


Figure 2. a) ¹H NMR spectrum of HYPAM4-DS100 in CHCl₃; b) and c) Selective 1D ¹H NOESY experiment with dodecyl sulphuric acid and HYPAM4-DS100 respectively in CDCl₃ after selective excitation of methylene group in α position of sulfate function (NOE mixing time : 800 ms).

In order to study the influence of structural parameters on the mesomorphic behavior, the level of functionalization of amine groups by DS was modified. Thus, four different ratios of

primary amine/sulfate groups were used: 1:1, 1:0.90, 1:0.75 and 1:0.5 leading to the formation of HYPAM-DS100, HYPAM-DS90, HYPAM-DS75 and HYPAM-DS50 respectively. ATR-FTIR spectroscopy was used to quantify the HYPAM4/DS proportions. Indeed, this molar ratio is proportional to the ratio of the intensity of the amide I band to the intensity of the sulfate bands. A calibration curve was obtained by measuring this ratio on spectra of the physical mixtures of HYPAM and SDS, for which the molar ratio of primary amine groups of HYPAM and SDS was varied from 1:1 to 1:0.5 (Figure S5 in ESI). Obtained results are reported in Table 2. A good agreement with theoretical expected values was observed for all studied compounds.

Additionally, complexes obtained with hyperbranched HYPAM of different molar masses or with the corresponding perfectly defined PAMAM dendrimers were synthesized with two targeted degree of functionalization: 90 and 100% (Table 2).

2.2. Thermal and mesomorphic properties. The mesomorphic behaviour of the dendritic complexes was studied by Differential Scanning Calorimetry (DSC), Polarizing Optical Microscopy (POM) and Small Angle X-ray Scattering (SAXS) experiments. Typical thermograms obtained are given in Figure 3 (see also Figure S6, S7, S26 and S27 in ESI). All transition temperatures and associated enthalpies are summarized in Table 2.

Table 2. Functionalization level and thermal characteristics of the different complexes determined by FT-IR and DSC measurements.

Compounds	DS/NH ₂ mol ratio [%]	C		LC		I
		T ₁ [°C]	(ΔH _C) [J/g]	T ₂ [°C]	(ΔH _{LC}) [J/g]	
HYPAM3-DS100	100 ^b	• 28.3 (17)	•	• 50.3 (0.6)	•	•
HYPAM4-DS100	97 ^a	• 23.5 (26)	•	• 48.8 (3.8)	•	•
HYPAM5-DS100	100 ^b	• 23.5 (20)	•	• 50.9 (4.0)	•	•
PAMAM4-DS100	99 ^a	• 24.0 (28)	•	• 47.2 (1.9)	•	•
PAMAM5-DS100	100 ^b	• 25.8 (24)	•	• 50.2 (2.3)	•	•
HYPAM4-DS50	51 ^a	-	-	-	-	-
HYPAM4-DS75	82 ^a	• 45.1 (15)	•	• 65.6 (1.3)	•	•
HYPAM4-DS90	95 ^a	• 23.3 (22)	•	• 52.5 (3.9)	•	•
PAMAM4-DS90	89 ^a	• 24.2 (24)	•	• 50.5 (2.8)	•	•
PAMAM5-DS90	90 ^b	• 24.5 (28)	•	• 48.7 (1.9)	•	•

^a estimated from FT-IR measurements (standard deviation ± 2),

^b estimated from experimental conditions.

For almost all complexes, glass transition temperature is barely or not visible. This may be ascribed to the high level of crystallinity of those complexes. This crystallinity is responsible of a first transition peak (at T₁) associated with a high variation of enthalpy and arises from the association of hydrophobic fatty chains.³² Additionally, for most of the dendritic structures, a second but less energetic transition is visible in the thermograms (T₂). Birefringent and different textures were observed by POM below T₁ and between T₁ and T₂ after which the material starts losing its birefringence suggesting the existence of two different liquid crystalline organizations of the studied materials (Figure 4). While no pre-mesogenic moiety is present in the polymer complexes, LC properties arise from a molecular segregation phenomenon between hydrophobic chains and the hydrophilic or

ionic part of the complexes.²³ This segregation necessitates a hydrophilic core of sufficient molar mass: thus ionic complexes between tris(2-aminoethyl)amine and DS does not exhibit mesomorphic properties. The observed textures could be ascribed to columnar (below T₁) and lamellar mesophases (between T₁ and T₂). The nature of these mesophases was clearly confirmed by SAXS measurements (*vide infra*).

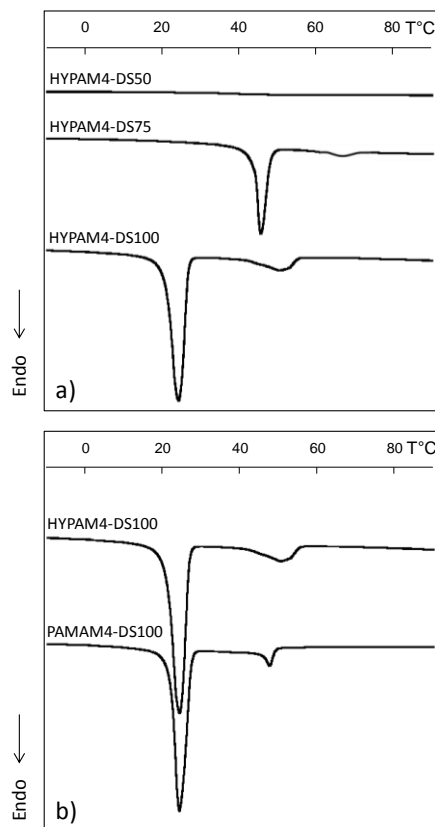
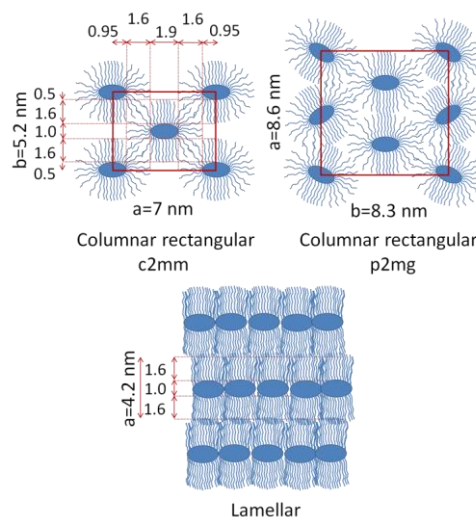


Figure 3. DSC thermograms recorded on heating at the rate of 10°C/min a) for HYPAM4 with 50, 75 and 100% level of functionalization with SDS and b) for HYPAM4 and PAMAM4 with a 100% level of functionalization.



Scheme 2. Schematic models of the rectangular columnar Col_{r,p2mg}, Col_{r,c2mm} and lamellar mesophases.

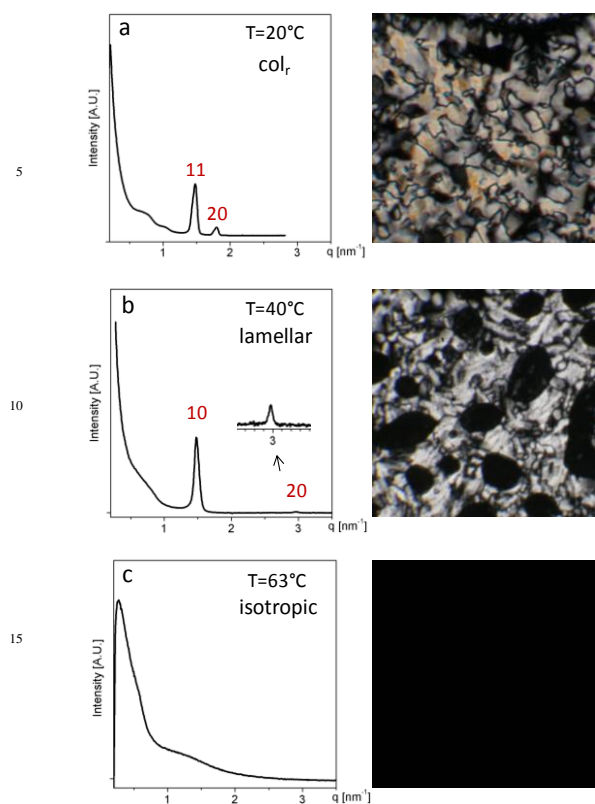


Figure 4. Diffraction intensity profile extracted from SAXS diffraction pattern for HYPAM4-DS100 at 20°C (Col_r), 40°C (SmA) and 63°C (Isotropic) and corresponding POM images.

Hence, HYPAM4-DS100 displayed two transitions temperatures at $T=23.5$ °C and 48.8 °C with an associated variation of enthalpy of 26 J/g and 3.8 J/g respectively (Figure 3 and Table 2). At temperatures lower than the first transition peak (i.e. 20°C), peaks at 1.45 and 1.80 nm^{-1} appeared on the radial averaged diffraction intensity profile extracted from the 2D SAXS diffraction pattern (Figure 4a). Those peaks could be ascribed to a rectangular columnar mesophase with $C2mm$ planar space group ($Col_r, C2mm$) and with lattice constants $a = 7.0$ nm and $b = 5.3$ nm (see Figure 4a and Table 3). The formation of such mesophase was previously observed by J.L. Serrano *et al.* for PAMAM derivative dendrimers.^{23,39} An arrangement for which the molecules are located at the centre and at the corners of the unit cell in such a way that the hydrocarbon chains segregate in layers could be proposed for this structure (see Scheme 2). By roughly estimating the contour length of fully stretched C_{12} alkyl tails to 1.6 nm and assuming no interdigitated alkyl chain configuration, an asymmetric domain size of 1×1.9 nm^2 can be estimated for hyperbranched domains. This value is in good agreement with both the expected and the observed values in literature.^{23,39} At the transition to the lamellar mesophase, the correlation along the columnar axis is lost due to the melting of crystalline structures leading to the disruption of the two-dimensional rectangular positional ordering. This was confirmed by SAXS measurements by the displacement of a sharp peaks in the wide angle region ($q=14-16$ nm^{-1} i.e. 4.2 Å) characteristics of the crystallinity of the surfactants domains at the first transition temperature (see Figure

S11 in ESI) towards low q regions at high temperature (i.e. toward a less organized system).³² Between the two transitions peaks, SAXS diffraction pattern showing three peaks $q_1:q_2:q_3$ (at 1.49, 2.98 and 4.47 nm^{-1}), spaced as 1:2:3 (Figure 4b and Figure S9 in supporting information), confirmed the lamellar nature of the liquid crystalline organization. The lattice parameter of the lamellar phase 4.2 nm corresponding to the width of hyperbranched and alkyl tails domains. Hence, a minimum width of 1.0 nm can be estimated for hyperbranched domains. Above T_c , both birefringence in POM and reflections of the LC in SAXS disappeared as expected for an isotropic phase (Figure 4c).

FT-IR allowed confirming previous results concerning the loss of crystalline order of SDS chains at the first transition temperature T_1 . Indeed, the CH_2 asymmetric and symmetric stretching vibrational frequencies can be used to describe the conformation of SDS molecules. The intensity of the signal relative to the CH_2 asymmetric stretching band was analyzed as a function of temperature (Figure 5). Interestingly, a significant jump was observed around 23°C, i.e. at the first transition temperature from columnar to lamellar mesophase. This suggests a strong change in SDS conformation at this transition temperature.⁴⁰ Furthermore, the separation between $\nu_{as}(SO_2)$ bands was an indication of the conformational structure of the surfactant.⁴¹ Values from 27 to 29 cm^{-1} were characteristic of the SDS crystalline conformation (all-*trans* conformation), from 39 to 48 cm^{-1} of SDS bulk and from 32 to 33 cm^{-1} of SDS liquid crystals.⁴¹ At 25°C, the band separation in our study is 28 cm^{-1} for crystalline SDS and for mechanical mixtures of HYPAM and SDS. This gap increases to 37 cm^{-1} for the complex. This also reflects a more disordered conformation in the lamellar phase than in the crystalline state. In addition, below T_1 the CH_2 asymmetric stretching band appears at 2917 cm^{-1} suggesting an ordered hydrocarbon chain in all-*trans* CH_2 configuration. The band shifts to a higher frequency at 25°C (2924 cm^{-1}) meaning that the number of all-*trans* conformers decreases and the number of gauche conformers of alkyl chain increases. This same value was found by Sperline for SDS molecules in a liquid crystal phase.⁴² Additional information about alkyl chain conformation is also obtained at the CH_2 scissoring mode, $\alpha(CH_2)$. A frequency around 1466 cm^{-1} and a band broadening is an indication of partially ordered conformation, which is associated with a less organized structure of SDS.

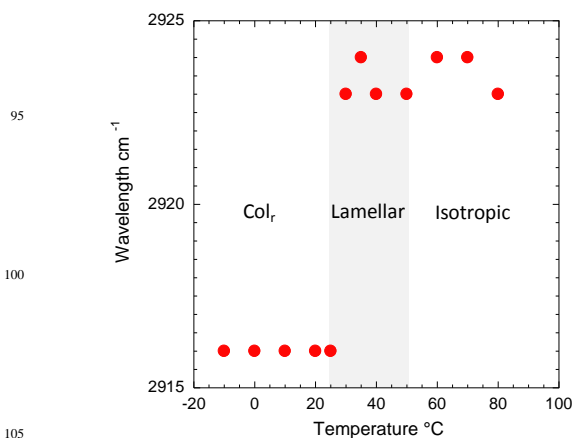


Figure 5. Thermal evolution of CH_2 asymmetric stretching band of HYPAM4-DS100 followed FT-IR.

Effect of structural parameters. The effects of molar mass, substitution level and architecture on the observed mesomorphic properties were hence systematically studied. Changing the molar mass of hyperbranched core poorly affects mesomorphous properties, as already reported in the literature.²³ Interestingly rectangular columnar mesophases were also identified below T₁ for HYPAM3-DS100 and HYPAM5-DS100 (see figures S8 and S10 in Supporting Information and Table 3). Nevertheless, in both cases a more complex 2D diffraction pattern suggested a mixture of a rectangular columnar mesophase with C2mm planar space group (Col_r,C2mm) and P2mg planar space group (Col_r,P2mg). Above the first transition temperature, a lamellar structure with structural parameter a = 4.2 nm was also identified. Once again, additional peaks depending on the thermal history of studied sample suggested partial ordering remaining within the lamellar structure. As shown in Table 3, lattice parameters were also not significantly modified by molar mass suggesting the predominant role of DS in the formation of such organized structures.

Table 3. Layer spacing and rectangular lattice constants determined by SAXS for the compounds at the indicated temperature

Compounds	T °C	Mesophase	Lattice parameters (nm)
HYPAM3-DS100	20	Col _r , p2mg	a=8.6, b=8.3
		Col _r , c2mm	a=7.0, b=5.3
	40	Col _{sq}	a=8.6
		Lamellar	a=4.2
HYPAM4-DS100	20	Col _r , c2mm	a=7.0, b=5.3
	40	lamellar	a=4.2
	63	Isotropic	
HYPAM5-DS100	20	Col _r , p2mg	a=8.6, b=8.3
		Col _r , c2mm	a=7.0, b=5.3
	40	Col _{sq}	a=8.6
		Lamellar	a=4.2
63	Isotropic		

Mesomorphic properties are more dramatically affected by changing the level of functionalization of amine terminal function as depicted in Figure 3a. Hence, T₁ and T₂ values increased from 23.5 to 45.1 °C and 48.8 to 65.6 °C respectively by decreasing the functionalization level from 97% to 82% (HYPAM4-DS100 and HYPAM4-DS75). As expected from the lower content of alkyl chain, the associated variation of enthalpy decreased accordingly. Interestingly, no mesomorphic behavior was observed when this level was decreased to 51% (HYPAM4-DS50). Lastly, a comparison of the mesomorphism of dendrimer based complexes and their hyperbranched counterpart with

similar molar masses allows demonstrating the effect of the dendritic architecture on the phase behavior. While transition temperatures were not significantly affected by this parameter (see Table 2 for the comparison of HYPAM4-DS100 with PAMAM4-DS100), the widths of the peaks corresponding to clearing temperature were shown to be significantly larger in the case of hyperbranched polymer. This effect is clearly seen in Figure 3b and may be ascribed to the larger dispersity of molar masses inherent for hyperbranched structures.

In conclusion, whereas LC properties of ionic complexes were not dependent on the molar mass of the hyperbranched functional cores, they significantly depended on the level of functionalization of the amine groups and to a lesser extent to the dendritic architecture. Interestingly, those structures presented a lamellar phase that could be taken into account either to control the growth of NPs within liquid crystalline phase or to obtain nanostructured materials as dispersed media. Both aspects will be described in the next section.

2.3. Behavior in solution and formation of polymeric aggregates. The ability of HYPAM-DS complexes to form colloidal solution was then evaluated. Due to their hydrophobic shell, the studied complexes were not soluble in aqueous and were only soluble in a very limited range of solvent (THF, chloroform, DMSO but not alkanes). The nature of solvent can dramatically affect the strength of interactions between the core and the shell. To characterize this effect and the aggregation phenomenon, we performed NMR and DLS studies in those solvents. Depending on the nature of solvent and its dissociative properties, these complexes presented different kinetics of dissociation as demonstrated by ¹H NMR. Hence, whereas in THF-d₈ HYPAM the core is barely visible, both peaks from HYPAM and DS appear as large peaks in CDCl₃ or DMSO-d₆ (Figure S12 in ESI) suggesting a different exchange mechanism in each case. In all cases, NOE transfer experiments demonstrated the interactions of DS ligands with HYPAM core in those solvents (see section 2.2). Nevertheless, based on DOSY experiments, a faster exchange mechanism may be assumed in the case of DMSO. The attribution of the peaks was carried out by one-dimensional ¹H and ¹³C NMR and two-dimensional ¹H-¹H COSY, ¹H-¹³C HSQC, experiments (Figures S13-S16 in ESI). A greater shift of the proton signal at 2.51 ppm to 3.37 ppm corresponding to the protonation of the primary amine in CH₂NH₂ group was observed. The shift from 2.24 ppm to 2.66 ppm of the signal of the methylene in α of tertiary amines (NCH₂CH₂NH₂) revealed that tertiary amines were also protonated. The chemical shifts for the other protons are weakly modified in HYPAM4 and in its corresponding complexes.

In addition, self-diffusion coefficients of HYPAM4, HYPAM4-DS100 and SDS were evaluated in DMSO solution at 308 K using the Pulsed-Gradient Spin-Echo (PGSE) NMR technique (Figure S17 in ESI). The obtained results are summarized in Table 4. Due to the large difference of hydrodynamic volume, HYPAM4 and SDS species exhibit a great difference in diffusion coefficients (10⁻¹⁰ and 2.6·10⁻¹⁰ m²·s⁻¹ respectively). In the case of HYPAM4-DS100 complex, two diffusion peaks were observed with smaller diffusion constants than for DS and HYPAM4 taken separately. This confirmed the formation of a complex with fast exchange mechanism in DMSO with respect to the time scale of

diffusion ($d_{20}=120\text{ms}$). Indeed only one diffusion coefficient was observed when PGSE NMR analysis was performed in THF-d8 which is a less dissociative solvent. From these values, the hydrodynamic radius (R_h) of the different components was calculated by means of the Stokes-Einstein equation. Both values were reported in Table 2 as well as hydrodynamic radius evaluated from DLS measurement (Figure S18 in ESI). R_h value was calculated from the D value for the complex is in accordance with those obtained by dynamic light scattering (DLS) measurement (i.e. 2.7 nm see Table 4).

Table 4. Self-diffusion coefficients and hydrodynamic radius (R_h) of SDS, HYPAM4 and HYPAM4-DS100 obtained by PGSE NMR and DLS.

Compounds	Diffusion coefficient ($\text{m}^2\cdot\text{s}^{-1}$)	R_h (nm) PGSE NMR	R_h (nm) DLS
SDS ^a	$2.6\cdot 10^{-10}$	0.5	-
HYPAM4 ^a	$1\cdot 10^{-10}$	1.4	-
HYPAM4-DS100 ^a	$0.5\cdot 10^{-10}$ $1.8\cdot 10^{-10}$	n.d. ^d	2.3 ± 1.1
HYPAM4-DS100 ^b	$1.1\cdot 10^{-10}$	4.3	2.7 ± 0.9
DMSO ^c	$6.5\cdot 10^{-10}$		

^a measured in DMSO (0.1 wt% polymer solution); ^b measured in THF (0.1 wt% polymer solution); ^c measured in DMSO or THF; ^d Ionic complex cannot be isolated in DMSO, thus R_h were not calculated in this solvent.

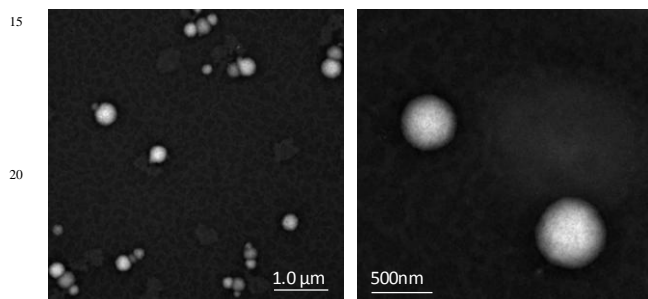


Figure 6. Representative TEM images of HYPAM4-DS100 samples stained with uranyl acetate of aggregates obtained in DMSO/water 3/1 v/v solution.

The formation of organized structures (see 2.2) as well as the amphiphilic structures of those ionic complexes may lead to the formation of structured aggregates in solution. Hence, JL. Serrano and coll. have previously observed the formation of spherical aggregates from hyperbranched mesomorphic structures favored by the pristine liquid crystalline organization.²³ In our case, HYPAM4-DS100 was dissolved in a good solvent DMSO at a concentration of 0.5 wt%. As shown above, by NMR measurements, HYPAM4-DS complexes are soluble in those conditions and a rearrangement of ligand is still possible while preserving ionic interactions. Milli-Q water, which was a poor solvent, was then added very slowly ($\sim 10\mu\text{L}\cdot\text{min}^{-1}$) to the complex solution in DMSO (1.5 mL) with slight shaking (final volume water content around 25%). The nature of the formed aggregates was examined by transmission electron microscopy

(TEM) with negative staining. Those objects with approximately spherical shape possessing the features of spheres were obtained as shown in Figure 6. As described in literature, these structures may arise from a lamellar organization where hydrophobic aliphatic chains are wrapped by the hydrophilic dendrimer core forming well-packed layers in which all the alkyl chains are oriented parallel to each other.

2.4. In situ formation of gold NPs. The ability of those mesomorphic ionic complexes to act as template for the formation of gold nanoparticles was then evaluated. As stated above, the development of an *in-situ* procedure to generate NPs within a LC medium has proved to be quite a challenging task.⁴ This is mainly due to two main factors. The first one is related to the difficulties to obtain homogeneous medium from the mixture of LC and NPs precursor. We previously pointed out the importance of such interactions to control growth mechanism of ZnO NPs.^{11,12} In that context the use of thermotropic structures comprising ionic counterpart facilitating interactions with ionic metal precursor to insure the homogeneity of hybrid materials before the formation of NPs. The second one is related to diffusion hindrance of reactants that induce the formation of NPs in such medium. Concerning this point, most studies involved the *in-situ* reduction of metal precursors *via* oxidation of the LC medium in order to obtain the desired NPs.^{9,13,14} In other cases, sputtering or electrodeposition techniques were used.^{8,15} Here a flux of dihydrogen will be used to ensure the reduction of the gold salt at the chosen temperature without disturbing mesomorphic order. So our first purpose is to evaluate if such ionic LC polymers 1) could lead to the formation of homogeneous medium prior to the formation of NPs and 2) could allow synthesizing well defined hybrid materials made of monodisperse NPs. The effect of polymer structure and organization on the morphology of gold nanoparticles will also be evaluated.

As a model system, we chose to study the formation of gold NPs. Their synthesis was performed either in the columnar phase (20 °C), lamellar phase (30 or 40°C) or in the isotropic state (50 and 65°C) to evaluate the effect of liquid crystalline organization on the NPs growth process. At each temperature a homogeneous mixture of ionic complexes and gold salt was obtained by crushing salt precursor with LC ionic polymer. Interactions between HAuCl_4 and HYPAM were evidenced by ^1H NMR experiments in D_2O solution: the addition of HAuCl_4 to a neutral polymer induced a shift of chemical shifts only for protons of primary and tertiary amines (an upfield shift of $\text{NCH}_2\text{CH}_2\text{NH}_2$ and a downfield shift of CH_2NH_2) (Figure S19 in ESI). Thus, metal ions can be coordinated to the outer primary as well as tertiary polymer amine groups. First attempts to obtain NPs by *in-situ* reduction of HAuCl_4 , 3 H_2O *via* direct oxidation of the LC medium due to the presence of amine function^{36,37} led to the formation of polydisperse gold NPs (Figure S28 in ESI). The kinetics of their formation was also found very slow: several hours are necessary to fulfil complete NPs formation as stated by measurement of absorbance of the growing NPs. Decreasing the dispersity of gold NPs is mandatory in order to assess precisely the effect of LC organisation on gold NPs formation. For this purpose, reduction of the bulk systems was obtained by using a flux of hydrogen. Reduction occurs in a few seconds as stated by

the slight change color of the hybrid materials. The formation of gold nanoparticles was first evidenced by UV measurements on the bulk materials by the appearance at 550 nm of a characteristic band corresponding to a surface plasmon (Figure S20 in ESI). The formed nanoparticles were further analyzed by TEM. Figure 7 and Figure 8 depicted TEM results obtained for Au NPs growth within HYPAM4-DS100 at five different temperatures (see also Figure S21 in ESI).

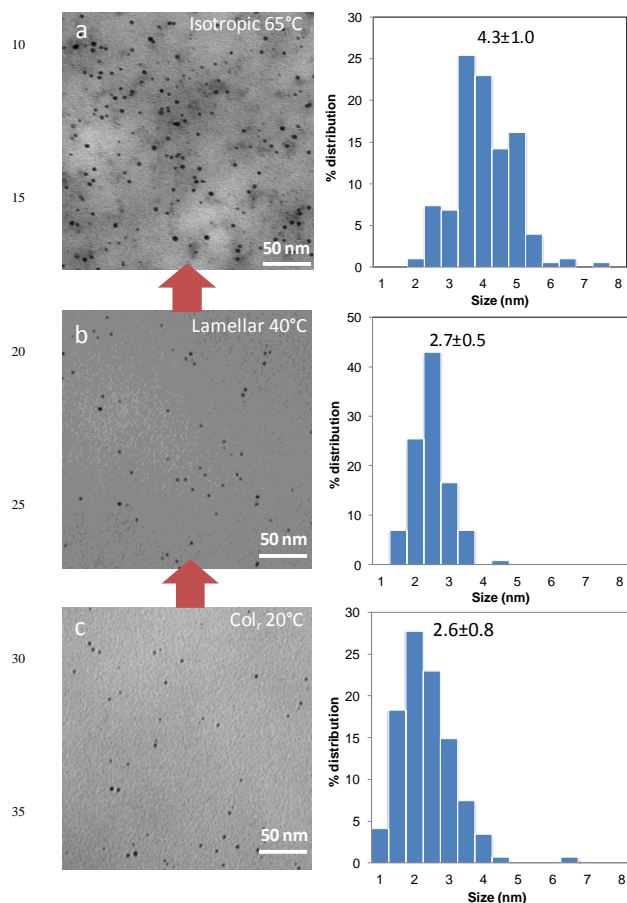


Figure 7. TEM micrographs of AuNPs synthesized either a) in isotropic conditions at 65°C or b) in a lamellar liquid crystalline state at 40°C or c) in a rectangular columnar state at 20°C, with corresponding size distributions.

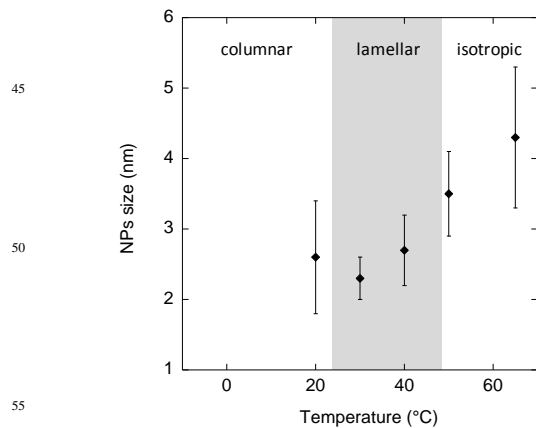


Figure 8. Effect on gold nanoparticle size of the temperature used during NPs synthesis. Liquid crystalline range corresponds to the one of mesomorphic polymer HYPAM4-DS100 before reduction.

A rather uniform distribution of particles throughout the sample was obtained either in the isotropic or in the LC states. This confirms the homogeneous character of the mixture prior to the reduction process. Interestingly, the obtained particles were smaller with a narrower distribution when growth of the particles occurred in the LC phases rather than in the isotropic state. Hence NPs size of 2.6 ± 0.8 , 2.3 ± 0.3 and 2.7 ± 0.5 nm were obtained at 20, 30 and 40°C respectively. At 50°C corresponding to the liquid crystalline to isotropic transition a slight but significant increase of NPs size at 3.5 ± 0.8 was observed. This increase in the isotropic state was further confirmed at 65°C for which NPs size of 4.3 ± 1.0 nm were found. Hence, as no difference in size was observed between 20 and 40°C, the effect of temperature could not alone explain the effect observed on NPs size. In addition an effect of the macromolecular organization should participate to this effect. To understand these results, we can assume that the main factor controlling the formation of gold particles is the diffusion of gold ions through the sample. Through electrostatic interactions between ammonium groups and the anionic gold salt, a preferential distribution of gold precursor within the ionic part of the complexes could be expected before reduction. The formation of gold NPs within LC structure may hence favour the formation of smaller Au NPs due to a better controlling diffusion of ionic species through hydrophilic regions of the lamellar phase. Formation of those NPs in the isotropic state facilitated diffusion of gold ions in all directions and thus increased the size of nanoparticles.

Nevertheless, NPs obtained either in the columnar or the lamellar phase presented similar sizes. To understand this, the mesomorphic behaviour of the synthesized bulk HYPAM4-DS/Au hybrids was assessed. For the hybrid materials synthesized at 30°C, upon hybridization of HYPAM4-DS100 with AuNPs, the first transition temperature corresponding to the transition from the columnar to the lamellar mesophase disappeared and only the second transition corresponding to the clearing temperature at 49.2°C remained. This value as well as the associated enthalpic variation is not significantly different from the one of pristine polymer (48.8°C). Thus while preserving LC properties over a similar temperature range, AuNPs strongly disturbed the organisation of hyperbranched polymer preventing the formation of the highly organized columnar mesophase. This results in the appearance of a glass transition temperature at 3.3 °C. A strong birefringence, with a texture characteristic of a lamellar mesophase was observed up to the clearing temperature. SAXS experiments performed at 20°C and 60°C support well this assumption (see Figure S22 in ESI) with almost complete disappearance of signals arising from columnar mesophase at 20°C (0.8 and 1.4 nm^{-1}). Disappearance of columnar mesophase may occur during NPs formation explaining the similar NPs size obtained regardless of the nature of the pristine LC phase. As expected, larger NPs obtained in isotropic conditions disturbed more strongly mesomorphic organization: thus, as can be seen on the thermogram, clearing temperature decrease to 40°C for the nanohybrids synthesized at 50°C (see Figure S23 in ESI).

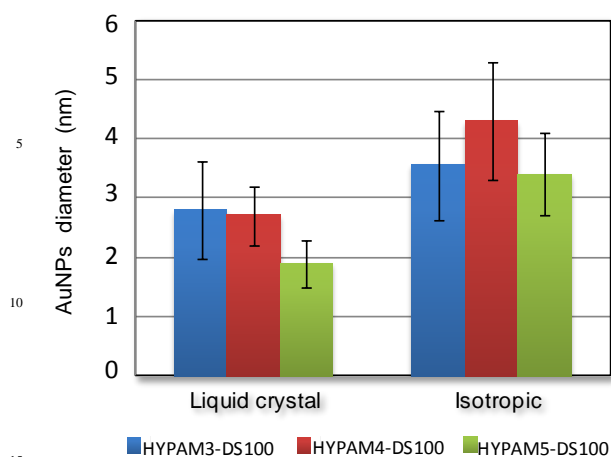


Figure 9. Histograms depicting the effect a) of the molar mass of the hyperbranched complex and b) of the polymer organization (lamellar or isotropic) on the Au NPs mean diameter.

To further analyze the effect of molecular architecture on the formation of gold NPs, the same set of experiments was performed with HYPAM3-DS100 and HYPAM5-DS100. As shown in Figure 9, similar results than the previous ones were obtained regardless of the molar mass of the hyperbranched structure. It has to be noted that a small but significant decrease of AuNPs size was obtained when increasing the molar mass of the complex (see also Figure S24 and S25 in ESI). This better control may be related to an increase of viscosity of the liquid crystalline phase. Such an effect has already been described to be a key parameter in previous studies leading in some cases to the formation of anisotropic structures.^{11, 12} Hence mesomorphic ionic hyperbranched polymers allow the formation of homogeneous medium comprising gold salt in LC medium. Its reduction led to gold NPs with low dispersity in size. Moreover, both structural parameters of the LC hyperbranched polymers and organization of the LC medium allow controlling the size of gold NPs.

3. Conclusion

Branched thermotropic liquid crystals were successfully obtained from the ionic interactions between hyperbranched polyamidoamine and sodium dodecylsulfate. These complexes present columnar rectangular and lamellar thermotropic mesophases as demonstrated by polarizing optical microscopy, differential scanning calorimetry, and small-angle X-ray scattering. The relationships between the structural characteristics of the polymers (size of the hyperbranched core, hyperbranched or dendritic nature of the core, substitution ratio) and the mesomorphic properties were studied. The liquid crystalline phase was then used for the *in situ* formation of gold nanoparticles. The templating effect of the liquid crystal mesophase resulted in the formation of isotropic nanoparticles, the size of which was dictated by the local organization of the mesophase and by the molar mass of the hyperbranched complex. The presence of NPs induced strong changes in local organization of the LCs polymer, but nevertheless the obtained hybrid materials remained liquid crystalline. To conclude, we believe

that such ionic complexes allowing strong interactions with inorganic materials precursors of different nature present promising opportunities for the formation of homogeneous hybrid materials within original thermotropic structures.

4. Experimental section

4.1. Materials.

Methylacrylate, tetrachloroauric acid trihydrate ($\text{HAuCl}_4 \cdot 3\text{H}_2\text{O}$), amine-terminated PAMAM dendrimers (G3 to G5) as methanol solutions were purchased from Aldrich and were used without further purification. For PAMAM solutions, methanol was removed under vacuum prior to use. Sodium dodecyl sulfate was also purchased from Aldrich and purified by recrystallisation in ethanol/water 95 v/v before use. Tris(2-aminoethyl)amine (Aldrich) was distilled under reduced pressure and stored under argon atmosphere before use. Ultrapure water ($\rho=18 \text{ M}\Omega \text{ cm}^{-1}$) from Aquadem apparatus was used for complex preparation.

4.2. Synthesis.

The synthesis of the HYPAM3, 4 and 5 cores were carried out following previously published work by our group^{34,35} For HYPAM4, 2.5 g of tris(2-aminoethyl)amine (17.1 mmol) were mixed with 1.13 g of tris(2-di(methylacrylate)aminoethyl)amine (1.7 mmol). The solution was stirred under argon atmosphere at 75°C during two days, at which time the products were dissolved in 5 mL CH_2Cl_2 and precipitated into 200 mL THF at 0°C. 2.05 g of precipitated polymer was obtained as a yellow gum. tris(2-di(methylacrylate)aminoethyl)amine was as followed. To 5.3 g of methylacrylate (61.6 mmol) in 6.5 mL of methanol was added dropwise a solution of 1.25 g of freshly distilled tris(2-aminoethyl)amine (8.5 mmol) in 1.5 mL of methanol at 0°C under argon atmosphere. The mixture was then stirred at room temperature during two days. The product (5.9 g) was obtained, after elimination of the solvent under vacuum, as a slightly yellow oil and used without further purification steps. HYPAM4: ¹H NMR (DMSO-d₆, 500 MHz): 2.24 (m, N-CH₂-CH₂-N); 2.45 (m, CO-NH-CH₂-CH₂-N); 2.51 (DMSO and m, -CH₂-NH₂); 2.63 (m, N-CH₂-CH₂-CO); 2.7 (m, N-CH₂-CH₂-CO); 3.1 (m, -CH₂-NH-CO-); 3.45 (NH); ¹³C NMR (DMSO-d₆, 500 MHz): 33.79 (N-CH₂-CH₂-N); 37.34 (-CH₂-NH-CO-); 41.62 (N-CH₂-CH₂-CO); 46.15 (-CH₂-NH₂); 47.43 (N-CH₂-CH₂-CO); 56.61 (CO-NH-CH₂-CH₂-N); 172.0 (CO); IR (HYPAM4): $\bar{\nu} = 3345, 3283, 3078, 2943, 2858, 2824, 1645, 1557, 1460, 1354, 1291, 1096, 1062, 946, 915 \text{ cm}^{-1}$; IR (SDS): $\bar{\nu} = 2956, 2918, 2851, 2872, 1468, 1250, 1222, 1096, 1082, 1017, 996, 831 \text{ cm}^{-1}$. The preparation of hyperbranched polymer surfactant complexes PAMAM-DS and HYPAM-DS was performed using PAMAM 3, 4 and 5 and HYPAM 3, 4 and 5 cores respectively. The grafted degree of SDS on polymers was calculated using the molar ratio of primary amine groups of the core on sulfate groups of SDS (ie 1:1, 1:0.75, 1:0.5). For example, the synthesis of HYPAM4-DS100 was carried out as follows: 25 mL of HYPAM4 acidic aqueous solution (pH 3-4) was prepared by slowly adding acidic solutions (HCl 0.1M and 0.001M) to 100 mg (0.62 mmol of NH₂ groups) of polymer. Then 7.95 mL of an acidic aqueous solution of SDS (0.078 mol.L⁻¹, concentration < cmc) at the same pH was added dropwise to the HYPAM solution under continuous stirring. Progressively, the obtained solution became turbid and the formed precipitate was isolated by centrifugation (8000 rpm,

20°C, 30 min). Then the residue was washed three times with water (3 x 20 mL) and dissolved in a small quantity of DMSO (1 mL). This organic solution was then added dropwise to 50 mL of an acid aqueous solution (HCl, pH3). The formed precipitate was collected by centrifugation (8000 rpm, 20°C, 30 min). The residue was washed by ultrapure water (40 mL) and centrifuged (8000 rpm, 20°C, 30 min) three times before dried under vacuum at room temperature for 3 days (251.22 mg, yield 94.7%). HYPAM4-DS100: ¹H NMR (500MHz, DMSO-d₆): 0.85 (t, ³J = 6.5 Hz, CH₃ alkyl chain); 1.24 (m, (CH₂)₉); qt (1.51, ³J=6.5 Hz, CH₂β); 2.51 (DMSO and m, N-CH₂-CH₂-NH-CO); 2.66 (m, N-CH₂-CH₂-N, N-CH₂-CH₂-CO); 2.91 (m, N-CH₂-CH₂-CO-); 3.20 (m, -CH₂-NHCO-); 3.37 (m, -CH₂-NH₃⁺; t, ³J=6.5 Hz, CH₂α); 3.52 (br M, NH) ppm; 3.74 (t, ³J=6.5 Hz, CH₂α); ¹³C-NMR (500 MHz, DMSO-d₆): 13.92 (CH₃); 22.15, 25.57, 28.80, 28.92, 29.10, 29.13, 29.16, 34.41 (CH₂ alkyl chain); 29.18 (CH₂β); 29.44, 50.60 (N-CH₂-CH₂-CO); 36.65, 43.85 (-CH₂-NH-CO-), 36.81 (N-CH₂-CH₂-N); 48.97 (-CH₂-NH₃⁺); 50.61 (N-CH₂-CH₂-CO); 52.01 (N-CH₂-CH₂-NHCO), 60.75 and 66.23 (CH₂α); 169.33 (CO) ppm; IR (HYPAM4-DS100 complex): $\bar{\nu}$ = 3484, 3291, 3084, 2956, 2924, 2853, 1660, 1557, 1466, 1390, 1379, 1241, 1204, 1057, 983, 804 cm⁻¹.

Synthesis and characterization of gold nanoparticles in mesophases. *In situ* synthesis of gold nanoparticles inside LC or isotropic HYPAM-DS was performed as followed: 500 μL of a 10⁻² mol.L⁻¹ HAuCl₄ solution in methanol was slowly evaporated in a mortar, after which 10 mg of the chosen hyperbranched ionic complex were added. The mortar was placed in a thermostated box at the desired temperature and the two components were well crushed with the thermostated pestle to obtain a homogeneous mixture. A flux of dihydrogen was added during 30s to assure the reduction of the gold salt (P(H₂) = 1 bar). The formed nanoparticles were analyzed by TEM.

4.3. Characterization of polymers and nanoparticles.

Nuclear Magnetic Resonance. To determine the structural characteristics of the polymers, NMR experiments were performed at 298K (or 308K in dmsO-d₆) on a Bruker AVANCE 500 MHz spectrometer equipped with a 5 mm Z-gradient TCI cryogenic probe. The 90° pulse length was 9 μs, the sweep width was 10kHz and the acquisition time was 3.5 s. The scan number was adjusted to obtain a sufficient signal to noise ratio and the relaxation delay between transients was 3s. For 1D ¹H experiments, a 30° pulse was used. Attribution of the signals was made by COSY, HSQC and HMBC experiments.

*Diffusion coefficient measurement by NMR-DOSY (Diffusion Ordered Spectroscopy).*⁴³ The basic scheme for the characterization of diffusion is the pulse field gradient spin-echo (PFGSE). The measurement was carried out by observing the attenuation of the NMR signals during a delay surrounded by two pulsed field gradients. In practice, a series of NMR diffusion spectra were acquired as a function of the gradient strength (g). The intensities of the resonances follow an exponential decay which depends on the self-diffusion coefficient (D).^{44, 45} Their relationship is given by the Stejskal-Tanner relation: $I/I_0 = \exp[\gamma^2 g^2 \delta^2 (\Delta - \delta/3) D]$ where I is the measured signal intensity, I₀ is the signal intensity for a g value of 0 G/cm, γ is the gyromagnetic ratio for the ¹H nucleus, δ is the gradient pulse length, Δ is the time between the two gradients in the pulse

sequence.⁴⁶ D values are function of temperature and viscosity as indicated from the Stokes-Einstein equation: $D = \kappa T / 6\pi\eta R_h$ (where k = Boltzmann constant, T temperature, η viscosity of the solution and R_h is the radius of the solvated species). The Z pulsed field gradients were generated with a 10 A GRASP II/P gradient amplifier. Thus, the z-maximum gradient strength (g) was 53.5 G/cm. Experiments were performed by varying g and keeping all other timing parameters constant. Typically, the Δ and the δ durations were 100 ms and 1ms, respectively and g was varied from 2.675 (strength of 5%) to 50.825 (strength of 95%) G/cm by 3% steps. An NMR pulse sequence with a stimulated echo bipolar gradient pulse pair and one spoil gradient was used (pulse program named stebpgp1s in the Bruker library). The data were analysed by maximum-entropy with the DOSY module of NMRnotebook software (NMRtec).⁴⁷ The DOSY processing algorithm parameter was set to 3 and the data were processed with a diffusion window from 0,1 to 25000 μm²/s.

Selective 1D ¹H NOESY Experiments. The nuclear Overhauser effect (NOE) between dipolar coupled ¹H nuclei is generally used in structural and conformational analysis of molecules and molecular interactions because its intensity is determined by the internuclear ¹H-¹H distance (r) according to an r⁻⁶ dependency and by the rotational correlation time (τ_c).⁴⁸ For a rigid spherical molecular complex with radius R and solvent viscosity η, τ_c is determined by the Stokes-Einstein relation: $\tau_c = 4\pi\eta R^3 / 3k_B T$. Owing to this relation, the NOE intensity signal of the ligand is dependent of its interaction with the macromolecules. The regime of the NOE changes from a small to a large molecule is related to the frequency of the spectrometer (ω) and the mobility of the molecules (τ_c). For ωτ_c = 1.1, zero intensity for NOE effects; for ωτ_c < 1.1, positive NOE signals; for ωτ_c > 1.1, negative NOE signals. In the case of ligand equilibrium between the nanoparticle surface (bound state) and the solution (free state), the NMR Transferred NOESY experiment could give some insights into this exchange rate. Indeed, for a given interaction time, the more the ligand is bound, the more the signal will be intense. Thus, to understand the interaction between ligand and nanoparticles, 1D ¹H selective NOE NMR experiments were used. Selective excitation was performed with double pulsed-field-gradient spin-echo scheme (DPFGSE) with a gaussian pulse shape.⁴⁹ The NOE mixing time was 800 ms. Other parameters were similar to those of 1D ¹H experiments.

Fourier transform infrared (FTIR). Spectra were recorded with a Nexus Thermo Nicolet spectrometer equipped with a detector DTGS, in attenuated total reflection (ATR) mode with a diamant crystal in the spectral region of 600-4000 cm⁻¹ with a resolution of 4 cm⁻¹. The physical mixtures were prepared by simple homogenization of HYPAM and SDS as followed: 25 mL of an aqueous solution of HYPAM (100 mg) was prepared. To this solution was added 7.95 mL, 7.15 mL, 6.36 mL, 3.98 mL of 0.078 mol.L⁻¹ aqueous SDS affording the 1:1, 1:0.80, 1:0.5 ratios respectively. The obtained solution was then freeze-dried and the spectra of the obtained solids were recorded. Reflexion IR spectra were recorded in a Microscope IN10MX ThermoFisher equipped with a detector MCT and connected to a LINKAM TMS 600. Spectral resolution of 8 cm⁻¹ was used and 16 scans were performed.

Differential Scanning Calorimetry. The crystallizations (T_c and

(T_{LC}) temperatures were determined by DSC using a Mettler Toledo DSC 1 STARe System Thermal Analysis calorimeter equipped with a Gas Controller GC200. Samples were sealed inside aluminum crucibles of 40 μ L in volume. Transition temperatures were taken at the top of the DSC peaks as the temperature increased at different rates; 10, 5, 2 and 1 $^{\circ}$ C/min, and finally extrapolated to 0 $^{\circ}$ C/min. The variation of enthalpy was measured as the temperature increased at a rate of 10 $^{\circ}$ C/min. Polarized Optical Microscopy (POM). Observation of LC textures was performed on a hot stage FP 82HT from Mettler Toledo under a polarized light optical microscope BX50 from Olympus. POM observations have been realized after heating samples in the isotropic state and slowly cooling to the aimed temperature. No specific treatment of glass plate was realized.

Small Angle X-ray Scattering. SAXS on samples was measured with a Nonius Rotating Anode Instrument (4 kW, Cu K α) with pinhole collimation and MARCCD detector (pixel size 79) and a distance of 74.4 cm between detector and sample, covering a range of the scattering vector $q = 4\pi\lambda^{-1}\times\sin(\theta)$ from 0.25 to 4.5 nm $^{-1}$ (2θ : scattering angle, $\lambda = 0.154$ nm). The observed scattering patterns were corrected for empty-beam scattering. The 2D diffraction patterns were transformed into a 1D radial average of the scattering intensity using the Fit2D software.

Transmission electron microscopy. TEM was performed on a MET Hitachi HT7700 transmission electron microscope operating at 200 kV accelerating voltage. To prepare samples for analysis, the mixture of nanoparticles and complex was dissolved in 1mL of DMSO. Samples for TEM were prepared by slow evaporation of droplets of colloidal solution deposited on a carbon-coated 200 mesh copper TEM grid (Ted Pella Inc.). The samples were then carefully dried overnight. The nanoparticle size-distribution histograms were determined by using magnified TEM images. The size distribution of the particles was determined by measuring a minimum of 200 particles of each sample. The size distributions observed were analyzed in terms of Gaussian statistics (wc (σ)).

Dynamic Light Scattering. DLS measurements were carried out with a Malvern Instrument Nano-ZS equipped with a He-Ne laser ($\lambda=633$ nm) on 0.1 wt% polymer solution. The correlation function was analyzed via the general purpose method (NNLS) to obtain the distribution of diffusion coefficients (D) of the solutes. The apparent diameter was then determined using the Stokes-Einstein equation. Mean diameter values were obtained from three different runs. Standard deviations were evaluated from diameter distribution.

Reflection UV measurements were conducted on an Ocean Optics system (DH 2000 FHS) equipped with Top Sensor Systems optical fibers (FCR-7UV200-2-1.5x100). Data were analyzed with Spectra Win from Ocean Optics.

Notes and references

^a IMRCP, Université de Toulouse, 118 route de Narbonne, 31062 Toulouse, France;

^b IMRCP, CNRS UMR 5623, 118 route de Narbonne, 31062 Toulouse Cedex 09, France

^c Department of Biomaterials, Max Planck Institute for Colloids and Interfaces, 14424 Potsdam-Golm, Germany

^d ICT, FR2599, Université de Toulouse, 118 route de Narbonne, 31062 Toulouse, France.

^e CMEAB, IFR-BMT, Université de Toulouse, 133 route de Narbonne, 31062 Toulouse, France.

*corresponding authors: viguerie@chimie.ups-tlse.fr and marty@chimie.ups-tlse.fr

† Electronic Supplementary Information (ESI) available: NMR, DSC, POM and SAXS data for hyperbranched complexes and associated hybrids. See DOI: 10.1039/b000000x/

Funding Sources

The authors acknowledge the CMEAB for TEM facilities and the EU for financial support on acquiring DSC apparatus (FEDER-35477 "Nanobjets pour la biotechnologie").

Acknowledgment

The authors thank Pascale Saint-Aguet for SEC measurements and Corinne Routaboul for FTIR measurements and fruitful discussions.

References

- H. K. Bisoyi and S. Kumar, *Chem. Soc. Rev.*, 2011, **40**, 306-319.
- T. Hegmann, H. Qi and V. M. Marx, *J. Inorg. Organomet. Polym. Mater.*, 2007, **17**, 483-508.
- G. L. Nealon, R. Greget, C. Dominguez, Z. T. Nagy, D. Guillon, J. L. Gallani and B. Donnio, *Beilstein J. Org. Chem.*, 2012, **8**, 349-370.
- S. Saliba, C. Mingotaud, M. L. Kahn and J. D. Marty, *Nanoscale*, 2013, **5**, 6641-6661.
- G. N. Karanikolos, P. Alexandridis, R. Mallory, A. Petrou and T. J. Mountziaris, *Nanotechnology*, 2005, **16**, 2372-2380.
- G. N. Karanikolos, P. Alexandridis and T. J. Mountziaris, *Mater. Sci. Eng. B*, 2008, **152**, 66-71.
- M. Groenewolt, M. Antonietti and S. Polarz, *Langmuir*, 2004, **20**, 7811-7819.
- W. Dobbs, J.-M. Suisse, L. Douce and R. Welter, *Angew. Chem. Int. Ed.*, 2006, **45**, 4179-4182.
- I. Gascon, J. D. Marty, T. Gharsa and C. Mingotaud, *Chem. Mater.*, 2005, **17**, 5228-5230.
- V. A. Mallia, P. K. Vemula, G. John, A. Kumar and P. M. Ajayan, *Angew. Chem. Int. Ed.*, 2007, **46**, 3269-3274.
- S. Saliba, Y. Coppel, M. F. Achard, C. Mingotaud, J. D. Marty and M. L. Kahn, *Angew. Chem. Int. Ed.*, 2011, **50**, 12032-12035.
- S. Saliba, Y. Coppel, C. Mingotaud, J. D. Marty and M. L. Kahn, *Chem. Eur. J.*, 2012, **18**, 8084-8091.
- A. Taubert, *Angew. Chem. Int. Ed.*, 2004, **43**, 5380-5382.
- A. Taubert, P. Steiner and A. Manton, *J. Phys. Chem. B*, 2005, **109**, 15542-15547.
- H. Yoshida, K. Kawamoto, H. Kubo, T. Tsuda, A. Fujii, S. Kuwabata and M. Ozaki, *Adv. Mater.*, 2010, **22**, 622-626.
- S. Saliba, P. Davidson, M. Imperor-Clerc, C. Mingotaud, M. L. Kahn and J. D. Marty, *J. Mater. Chem.*, 2011, **21**, 18191-18194.
- V. Chechik, M. Q. Zhao and R. M. Crooks, *J. Am. Chem. Soc.*, 1999, **121**, 4910-4911.
- A. G. Cook, U. Baumeister and C. Tschierske, *J. Mater. Chem.*, 2005, **15**, 1708-1721.
- C. F. J. Faul, M. Antonietti, H. P. Hentze and B. Smarsly, *Colloids Surf. A*, 2003, **212**, 115-121.
- C. F. C. Fite, I. Tomatsu, D. Byelov, W. H. de Jeu and R. P. Sijbesma, *Chem. Mater.*, 2008, **20**, 2394-2404.
- S. Hernandez-Ainsa, J. Barbera, M. Marcos and J. L. Serrano, *Chem. Mater.*, 2010, **22**, 4762-4768.
- S. Hernandez-Ainsa, J. Barbera, M. Marcos and J. L. Serrano, *J. Polym. Sci. Pol. Chem.*, 2011, **49**, 278-285.
- S. Hernandez-Ainsa, J. Barbera, M. Marcos and J. L. Serrano, *Soft Matter*, 2011, **7**, 2560-2568.
- S. Hernandez-Ainsa, M. Marcos, J. Barbera and J. L. Serrano, *Angew. Chem. Int. Ed.*, 2010, **49**, 1990-1994.
- M. Marcos, R. Alcalá, J. Barbera, P. Romero, C. Sanchez and J. L. Serrano, *Chem. Mater.*, 2008, **20**, 5209-5217.
- M. Marcos, R. Martin-Rapun, A. Omenat, J. Barbera and J. L. Serrano, *Chem. Mater.*, 2006, **18**, 1206-1212.

- 27 R. Martin-Rapun, M. Marcos, A. Omenat, J. Barbera, P. Romero and J. L. Serrano, *J. Am. Chem. Soc.*, 2005, **127**, 7397-7403.
- 28 R. Martin-Rapun, M. Marcos, A. Omenat, J. L. Serrano, E. T. De Givenchy and F. Guittard, *Liq. Cryst.*, 2007, **34**, 395-400.
- 5 29 S. Ujiie, M. Osaka, Y. Yano and K. Iimura, *Kobunshi Ronbunshu*, 2000, **57**, 797-802.
- 30 S. Ujiie, Y. Yano and A. Mori, *Mol. Cryst. Liq. Cryst.*, 2004, **411**, 1525-1531.
- 31 L. A. Bastardo, V. M. Garamus, M. Bergstrom and P. M. Claesson, *J. Phys. Chem. B*, 2005, **109**, 167-174.
- 10 32 N. Canilho, M. Scholl, H. A. Klok and R. Mezzenga, *Macromolecules*, 2007, **40**, 8374-8383.
- 33 J. D. Marty, E. Martinez-Aripe, A. F. Mingotaud and C. Mingotaud, *J. Colloid Interf. Sci.*, 2008, **326**, 51-54.
- 15 34 S. Saliba, C. V. Serrano, J. Keilitz, M. L. Kahn, C. Mingotaud, R. Haag and J. D. Marty, *Chem. Mater.*, 2010, **22**, 6301-6309.
- 35 P. R. Dvornic, J. Hu, D. J. Meier, R. M. Nowak and P. L. Parham, Hyperbranched Polyureas, Polyurethanes, Polyamidoamines, Polyamides and Polyesters. 2003, U.S. Patent 6,534,600 B2.
- 20 36 N. Perignon, J. D. Marty, A. F. Mingotaud, M. Dumont, I. Rico-Lattes and C. Mingotaud, *Macromolecules*, 2007, **40**, 3034-3041.
- 37 N. Perignon, A. F. Mingotaud, J. D. Marty, I. Rico-Lattes and C. Mingotaud, *Chem. Mater.*, 2004, **16**, 4856-4858.
- 38 D. R. Scheuing and J. G. Weers, *Langmuir*, 1990, **6**, 665-671.
- 25 39 J. M. Rueff, J. Barbera, B. Donnio, D. Guillon, M. Marcos and J. L. Serrano, *Macromolecules*, 2003, **36**, 8368-8375.
- 40 G. Palaprat, J. D. Marty, C. Routaboul, A. Lattes, A. F. Mingotaud and M. Mauzac, *J. Phys. Chem. A*, 2006, **110**, 12887-12890.
- 41 R. B. Viana, A. B. F. da Silva and A. S. Pimentel, *Advances in Physical Chemistry*, 2012, **2012**, 14.
- 30 42 R. P. Sperline, *Langmuir*, 1997, **13**, 3715-3726.
- 43 C. S. Johnson, *Prog. Nucl. Magn. Reson. Spectrosc.*, 1999, **34**, 203-256.
- 44 W. S. Price, *Concept. Magnetic Res.*, 1997, **9**, 299-336.
- 35 45 W. S. Price, *Concept. Magnetic Res.*, 1998, **10**, 197-237.
- 46 E. O. Stejskal and J. E. Tanner, *J. Chem. Phys.*, 1965, **42**, 288+.
- 47 M. A. Delsuc and T. E. Malliavin, *Anal. Chem.*, 1998, **70**, 2146-2148.
- 48 B. Fritzinger, I. Moreels, P. Lommens, R. Koole, Z. Hens and J. C. Martins, *J. Am. Chem. Soc.*, 2009, **131**, 3024-3032.
- 40 49 K. Stott, J. Keeler, Q. N. Van and A. J. Shaka, *J. Magn. Reson.*, 1997, **125**, 302-324.